

Multiple Auger decay following ionization-excitation of Ne I

Qing Liu¹, Zhenqi Liu¹, Yulong Ma² and Yizhi Qu^{1,*}

¹*School of Optoelectronics, University of Chinese Academy of Sciences, Beijing 100049, China*

²*College of Physics and Electronic Engineering, Northwest Normal University, Lanzhou 730070, China*

 (Received 3 April 2022; revised 4 July 2022; accepted 8 July 2022; published 25 July 2022)

The photoionization-excitation spectrum of Ne I, in which an electron in the $1s$ shell is ionized and the $2p$ orbital electron simultaneously excited to the np orbital, is investigated in detail for complex satellite states $\text{Ne}^+ 1s^{-1}2p^{-1}(^1,^3P)np$ ($n = 3, 4, 5, 6, 7$). Then, the multiple Auger decay process is studied using the multistep method, including cascade, knock-out, and shake-off mechanisms, based on perturbation theory for the satellite states $\text{Ne}^+ 1s^{-1}2p^{-1}(^1,^3P)np$ ($n = 3, 4$) with two holes. The major single Auger decay can be described as a spectator process that valence electrons remain in the original orbitals. For double Auger decay, direct and cascade processes are considered, in which the direct mechanism is dominated by the spectator process, while the cascade mechanism is mainly from the participator process. For triple Auger decay, the important contribution is from the process consisting of direct double Auger and the subsequent single Auger electron emissions. The calculated ion yields of Ne^{2+} , Ne^{3+} , and Ne^{4+} for multiple Auger process of satellite states $\text{Ne}^+ 1s^{-1}2p^{-1}(^1,^3P)np$ ($n = 3, 4$) are consistent with experimental values [Hikosaka *et al.*, *Phys. Rev. A* **97**, 023405 (2018)].

DOI: [10.1103/PhysRevA.106.012819](https://doi.org/10.1103/PhysRevA.106.012819)

I. INTRODUCTION

The photoionization-excitation process can produce a series of satellite states where the emission of electron in the inner shell is accompanied by the simultaneous excitation of a valence electron to the energetically allowed unoccupied shell. Satellite states having abundant atomic structures can also provide more important information on electron correlation [1,2], and the formation and decay mechanisms of them are expected to become a powerful tool for material analysis and chemical research [3,4]. The decay of inner-shell vacancy states can take place by Auger transition where the filling of the vacancy by the outer-shell electron is accompanied by the simultaneous emission of another outer-shell electron [5]. The Auger process will affect the degree of ionization, which is a decisive parameter for plasmas in laboratory ion sources, soft x-ray lasing based on inner-shell transitions in plasma, fusion reactors and in astrophysics [6,7].

Satellite or shakeup structure of atoms and molecules have been studied for several decades [8–12]. In terms of the experiment, using the x-ray photoelectron spectroscopy, the satellite states of rare-gas $\text{Ne}^+ 1s^{-1}$, $\text{Ar}^+ 2p^{-1}$, $\text{Kr}^+ 3d^{-1}$, and $\text{Xe}^+ 4d^{-1}$ were measured [8,13,14]. Becker *et al.* revealed Auger decay of a series of Ne satellite states by using a time-of-flight photoelectron spectrometer that promoted further development of the experiment [15]. The different generated channels of $\text{Ar}^+ 2p^{-1}$ satellite states in the photoionization-excitation process were measured by Sankari *et al.* [16]. However, it is a great challenge for the theorists to study the structures and decay mechanisms of them due to many-body correlation, and the configuration interaction (CI) method was used to study only the structure of satellite states, without

involving the decay mechanism [17,18]. In 2006, single Auger decay (SA) of $\text{K}^+(2p^{-1}4s^{-1}nl)$ were considered using multi-configuration Dirac-Fock method [19], and the structures of $\text{Si}^+ 2p^{-1}$ and $\text{Si}^+ 2s^{-1}$ satellite states were discussed by Jänkälä *et al.* and Partanen *et al.*, respectively, using the same method [20,21].

With the development of the experimental technology, the Auger decay of satellite states can be effectively isolated from photoionization using a magnetic bottle time-of-flight spectrometer [22–24]. In 2012, the different SA decay channels of $\text{Ar}^+ 2p^{-1}3p^{-1}np$ ($n = 4, 5, 6$) and $\text{Ar}^+ 2p^{-1}3s^{-1}4s$ were observed by Nakano *et al.* [25]. In 2018, the multiple Auger decay of $\text{Ne}^+ 1s^{-1}2p^{-1}np$ ($n = 3, 4$) was measured using the multielectron coincidence method by Hikosaka *et al.* [23]. In 2020, the interesting phenomenon was found that the satellite states $\text{Ne}^+ 1s^{-1}2s^{-1}nl$ ($nl = 3s, 3p$) firstly emit a slow electron while the deep vacancies remain spectator [26]. To the best of our knowledge, there are few theoretical works devoted to exploring the single Auger processes of the satellite states [19–21], and even fewer for multiple Auger decay; therefore, its research is highly expected.

In this work, the photoionization excitation processes of Ne I are investigated, in which the satellite states $\text{Ne}^+ 1s^{-1}2p^{-1}np$ are generated by ionizing a $1s$ electron and simultaneously exciting the $2p$ orbital electron to the np orbital. The energy position, relative intensity (the photoionization cross section of $\text{Ne}^+ 1s^{-1}$ is normalized to 1) and ratio B of satellite states $\text{Ne}^+ 1s^{-1}2p^{-1}(^3P)np$ ($n = 3, 4, 5, 6, 7$) are obtained. In the subsequent parts, the satellite states $\text{Ne}^+ 1s^{-1}2p^{-1}(^3P)np$ and $\text{Ne}^+ 1s^{-1}2p^{-1}(^1P)np$ are abbreviated as $\text{Ne}^+ (^3P)np$ and $\text{Ne}^+ (^1P)np$. Based on perturbation theory, the rates of SA, double Auger (DA), and triple Auger (TA) decay of the main satellite states $\text{Ne}^+ 1s^{-1}2p^{-1}np$ ($n = 3, 4$) are studied including indirect (cascade) and direct mechanisms by using the multistep method. The knock-out (KO) and shake-off (SO)

*yzqu@ucas.edu.cn

mechanisms have been used to deal with direct multiple Auger decay [27,28], direct ion-atom collision processes [29], which can successfully explain experiments, and they are used to investigate the direct multiple Auger process of satellite states in this work. Ion yield is an important parameter for studying the interaction of x rays and ultrafast x rays with atoms [30]. Our multiple Auger decay rates, the Auger electron spectra, and the ion yield are consistent with the experimental results [23].

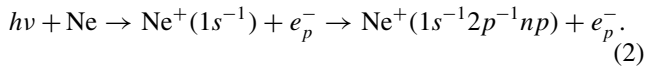
The subsequent arrangement of the paper is as follows. In Sec. II, the theoretical method is introduced. In Sec. III, the photoionization spectrum, the Auger electron spectrum, the Auger transition rates, and the BRs of different configurations as well as the ion yields are presented and discussed in detail. Lastly, a brief conclusion is given in Sec. IV.

II. THEORY

The multi-configuration Dirac-Hartree-Fock is a common and effective *ab initio* method for the calculation of multielectron atomic or ionic systems. The detail of this method was described by Grant [31], and is briefly introduced here. The atomic state functions

$$|\Gamma PJM\rangle = \sum_{i=1}^{n_c} c_{i\Gamma} |\gamma_i PJM\rangle \quad (1)$$

are obtained by a linear combination of configuration wave functions (CSFs). The P , J , and M are parity, electronic total angular momentum, and magnetic quantum number, respectively; $c_{i\Gamma}$ are the mixing coefficients that represent the interaction between CSFs, and γ is the other quantum number that defines uniquely CSF [32]. The CSF is antisymmetric functions obtained by the product of all-electron orbital wave function. Satellite states $\text{Ne}^+ 1s^{-1}2p^{-1}np$ are produced after an electron of $1s$ orbital is ionized, and a $2p$ orbital electron is simultaneously excited to the np orbital:



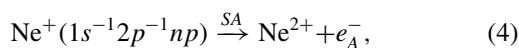
The generation of such complex satellite states is usually caused by the electron-electron interaction of the final states, and it is very important to consider the electron correlation effect.

Using the obtained wave function for neutral and satellite states, the photoionization cross section is calculated by dipole approximation:

$$\sigma_{\alpha\beta}(J_\beta M_\beta) = \frac{4\pi^2\alpha\omega}{3(2J_\alpha + 1)} \sum_{\kappa, J_T} |D(\omega; J_\beta M_\beta, \kappa : J_T M_T)|^2. \quad (3)$$

J_α and J_T are the total angular momentum of the initial state $|\psi_\alpha\rangle = |\psi(J_\alpha M_\alpha)\rangle$ and final state $|\psi_i\rangle = |\psi(J_\beta M_\beta, \kappa : J_T M_T)\rangle$, respectively, of satellite states $|\psi(J_\beta M_\beta)\rangle$ plus a photoelectron electron, and κ is the photoelectronic relativistic angular quantum number. To analyze the satellite states, in Eq. (3), the relaxation process of electrons was considered [24].

The SA transition process of satellite states can be expressed as



where e_A^- represent Auger electron. The corresponding transition probability is [27,28]

$$A_{\beta\gamma}^1 = \left| \langle \psi_\gamma^{2+}, \varepsilon_1 \kappa_1; J_{T_1} M_{T_1} | \sum_{i<j}^N \frac{1}{r_{ij}} | \psi_\beta^+ \rangle \right|^2, \quad (5)$$

where the $|\psi_\gamma^{2+}, \varepsilon_1 \kappa_1\rangle$ are the final states of Ne^{2+} , ε_1 and κ_1 are energies and angular quantum numbers of Auger electrons, respectively. J_{T_1} is the total angular momentum of final ionic states of Ne^{2+} coupling with the continuum Auger electron.

Generally, the DA process is divided into direct and indirect processes [33,34]. The direct DA (DDA) process assumes that two Auger electrons are emitted simultaneously, which can be shown as



In general, the DDA processes are handled by KO and SO mechanisms [35,36]. The KO mechanism can be considered as the electron impact ionization process between the intermediate Auger electron with energy ε_1 and intermediate states $|\psi_\gamma^{2+}\rangle$. The transition rate is [34,37]

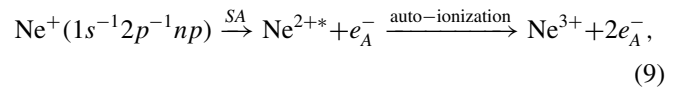
$$A_{\beta\delta(DK)}^2 = \sum_\gamma A_{\beta\gamma}^1 \Omega_{\gamma\delta}(\varepsilon_1), \quad (7)$$

where $A_{\beta\gamma}^1$ is the rate of SA process from satellite states to intermediate states of Ne^{2+} , $\Omega_{\gamma\delta}(\varepsilon_1)$ is the collision intensity due to the inelastic scattering of the intermediate Auger electrons with energy ε_1 . For the SO mechanism, because of the sudden change of atomic potential by the SA decay, two Auger electrons are emitted [33,35], then the transition rate can be expressed as

$$A_{\beta\delta(DS)}^2 = \sum_\gamma A_{\beta\gamma}^1 |\langle \psi_\delta^{3+}, \varepsilon_2 \kappa_2; J_{T_2} M_{T_2} | \psi_\gamma^{2+} \rangle|^2. \quad (8)$$

The states $|\psi_\delta^{3+}, \varepsilon_2 \kappa_2\rangle$ represent final states of Ne^{3+} , plus a continuum Auger electron with the relativistic angular quantum number κ_2 , $\langle \psi_\delta^{3+}, \varepsilon_2 \kappa_2; J_{T_2} M_{T_2} | \psi_\gamma^{2+} \rangle$ is overlapping integration due to relaxation effects between the ‘‘intermediate’’ states of Ne^{2+} and final states $|\psi_\delta^{3+}, \varepsilon_2 \kappa_2\rangle$ [33,38,39].

For the indirect DA process, it is usually assumed to be a cascade DA (CDA) process, as follows:



in which the satellite states $\text{Ne}^+ 1s^{-1}2p^{-1}np$ transition to the intermediate autoionization state of Ne^{2+} , which can decay further to the final state of Ne^{3+} by emitting two Auger electrons step by step. The expression of transition rate for CDA is as follows:

$$A_{\beta\delta(DC)}^2 = \sum_\gamma A_{\beta\gamma}^1 A_{\gamma\delta}^1 \Gamma_\gamma^{-1}, \quad (10)$$

where $A_{\gamma\delta}^1$ is the transition rate from the intermediate Ne^{2+} state $|\psi_\gamma\rangle$ to the final Ne^{3+} state $|\psi_\delta\rangle$, and Γ_γ represents the total decay rate of the intermediate state $|\psi_\gamma\rangle$.

In this work, the wave functions are calculated with the GRASP2K code [40]. The photoionization cross section and

rates of the SA process are obtained by the PHOTO component and the AUGER component of the RATIP-2012 program [41], respectively. The Flexible Atomic Code [33,42] is used to compute the impact ionization strength and overlapping integral for obtaining the rates of DDA and TA decay.

III. RESULTS AND DISCUSSION

In this section, the photoionization spectra of Ne I, the energy positions and intensities of various satellite states, Auger electron spectrum, and the ion yields for multiple Auger decay processes are obtained and analyzed in detail. The photoionization and Auger electron spectrum are obtained by convolving photoionization cross section and Auger rates with a Gaussian profile of specific full width at half maximum (FWHM), respectively, based on the energy resolving power of the spectrometer $E/\Delta E \sim 60$ in the experiment [23].

A. Ionization-excitation process of Ne I

For the photoionization-excitation processes, due to the rearrangement of electron density in the photoionization process of $1s$ shell, the shakeup processes of valence electrons $2p \rightarrow (3p, 4p, 5p, 6p, 7p)$ are induced. Then, the initial states of Ne I and final Ne^+ states were optimized separately [43,44], and the biorthogonal transformation between initial and final states is considered by using the biorthogonal component BIOTRA of the GRASP2K program [40]. For describing the structures of main states and the complex satellite states, the self-consistency procedures were performed for reference configurations $1s^2 2s^2 2p^6$ of Ne I and $1s^{-1}, 1s^{-1} 2p^{-1} 3p$ of Ne^+ ion to obtain orbital wave functions, respectively. The large-scale CI calculations are considered by including the configuration spaces of all single and double (SD) excitations from the reference configurations into $3s, 3p, 3d, 4s, 4p, 5p, 6p, 7p$, and $8p$ orbital. Our test calculations show that the configurations with higher states can be ignored.

The cross sections are revealed by the solid vertical lines at the bottom of Fig. 1. The photoionization spectrum is obtained

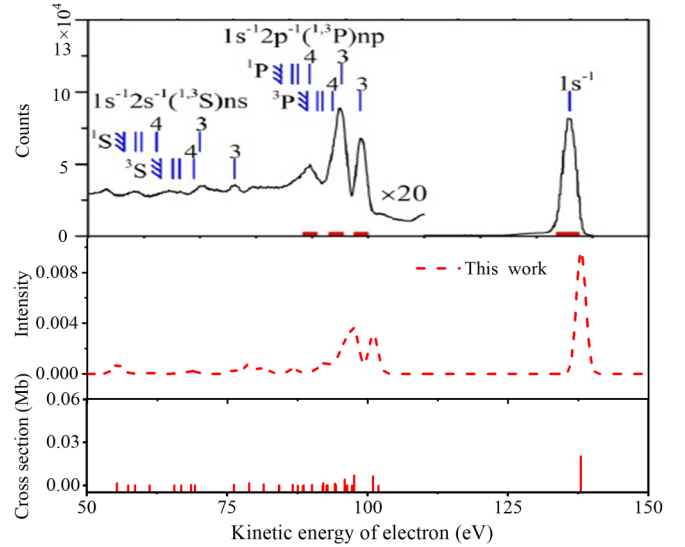


FIG. 1. Theoretical and experimental [23] photoionization spectra for Ne atom. The locations and intensities of main states $1s^{-1}$ and its satellite states are indicated with vertical bar in the bottom.

by convolving the cross sections with a Gaussian profile of 2-eV FWHM for the energy of photoelectron around 120 eV, and agree with the experimental spectra [23]. For the satellite states, it is found that the main peak around 96 eV contained the states $\text{Ne}^+ ({}^1\text{P})3p$ and $\text{Ne}^+ ({}^3\text{P})4p$, the former makes the main contributions. It can be seen from Fig. 1 that Ne^+ ions have abundant satellite structures with two vacancies. The satellite states $\text{Ne}^+ 1s^{-1} 2s^{-1} ({}^{1,3}\text{S})ns$ ($n = 3, 4$) are not considered in this work, since their intensities are one order of magnitude smaller than those of $\text{Ne}^+ ({}^{1,3}\text{P})np$.

It should be noted here that for comparison with experimental [45] and other theoretical results [46], the relative intensity (the photoionization cross section of $\text{Ne}^+ 1s^{-1}$ is normalized to 1), energy positions of complex satellite states $\text{Ne}^+ ({}^{1,3}\text{P})np$ are listed in Table I. For the energy positions,

TABLE I. The energy and intensity relative to that of $\text{Ne}^+ 1s^{-1}$ state for satellite states $\text{Ne}^+ 1s^{-1} 2p^{-1} ({}^{1,3}\text{P})np$ and ratio B are compared with theoretical (Theo.) [46] and experimental (Expt.) results [45]. The ratio B represents the proportion of the intensity to the total satellite states intensity; n represents the principal quantum number of valence electrons.

| | n | Relative energy (eV) | | Intensity (%) | | | Ratio B (%) | | |
|--|-----|----------------------|-----------|---------------|-----------|-------|---------------|-----------|-------|
| | | Expt. | This work | Expt. | This work | Theo. | Expt. | This work | Theo. |
| $\text{Ne}^+ 1s^{-1} 2p^{-1} ({}^3\text{P})np$ | 3 | 37.30 | 37.17 | 3.27 | 2.86 | 1.07 | 31 | 31 | 16 |
| | 4 | 42.30 | 42.08 | 1.90 | 1.53 | 1.34 | 18 | 17 | 20 |
| | 5 | 44.06 | 43.81 | 0.50 | 0.53 | 1.05 | 5 | 6 | 15 |
| | 6 | 45.02 | 44.73 | 0.30 | 0.35 | | 3 | 4 | |
| | 7 | | 45.91 | | 0.11 | | | 1 | |
| | >7 | | | | 0.02 | | | ~0 | |
| $\text{Ne}^+ 1s^{-1} 2p^{-1} ({}^1\text{P})np$ | 3 | 40.71 | 40.75 | 3.15 | 2.08 | 1.60 | 29 | 23 | 23 |
| | 4 | 46.39 | 45.92 | 1.20 | 1.00 | 1.27 | 11 | 11 | 19 |
| | 5 | 48.41 | 48.86 | 0.40 | 0.42 | 0.50 | 4 | 5 | 7 |
| | 6 | 49.45 | 49.41 | | 0.16 | | | 2 | |
| | 7 | | 51.90 | | 0.09 | | | 1 | |
| | >7 | | | | 0.01 | | | ~0 | |

our results are consistent with the experimental ones [45], in which the maximum difference is 0.47 eV corresponding to the satellite states $\text{Ne}^+ ({}^1\text{P})4p$. For the intensities, the satellite state $\text{Ne}^+ ({}^1\text{P})6p$ is observed in the experiment, while its intensity is not given in the literature due to the mixing with $\text{Ne}^+ ({}^1\text{P})7p$ [45]. In this work, the intensities of satellite states $\text{Ne}^+ ({}^{1,3}\text{P})np$ ($n = 3, 4, 5, 6, 7$) are obtained. Since both our and experimental intensities [45] of satellite states $\text{Ne}^+ ({}^{1,3}\text{P})np$ are relative to that of $\text{Ne}^+ 1s^{-1}$ state, for comparison, the intensities given in Table 4 of Ref. [46] have been divided by that of the main line. As shown in Table I, compared with experimental results [45], the present intensities of satellite states $\text{Ne}^+ 1s^{-1}2p^{-1}({}^{1,3}\text{P})np$ are better than those obtained by Kiselev *et al.* [46] with the nonrelativistic L-S (L represent the orbital angular momentum and S represent spin angular momentum) coupling approximation method. It should be pointed out that satellite states are sensitive to electron correlations; therefore, the configuration space of Kiselev *et al.* [46] less than ours may be the main reason for the difference in results. Although the relative intensity of $\text{Ne}^+ ({}^3\text{P})np$ and $\text{Ne}^+ ({}^1\text{P})np$ series are slightly smaller than the experimental values [45], the ratios of lower $\text{Ne}^+ ({}^3\text{P})np$ series to upper $\text{Ne}^+ ({}^1\text{P})np$ ones are 1.04, 1.53, and 1.26 for $n = 3, 4, 5$, which are consistent with experimental [45] results of 1.37, 1.58, and 1.25, respectively. It is because the $\text{Ne}^+ ({}^1\text{P})np$ ($n > 4$) are autoionization states with Fano resonances; then, the experimental intensities of $\text{Ne}^+ ({}^1\text{P})4p$ and $\text{Ne}^+ ({}^1\text{P})5p$ have a certain deviation, which is explained in the literature [45]. Also shown in Table I, the contributions of $\text{Ne}^+ ({}^{1,3}\text{P})np$ ($n > 7$) are much smaller than that of $\text{Ne}^+ ({}^{1,3}\text{P})7p$; therefore, the contributions of satellite states $\text{Ne}^+ ({}^{1,3}\text{P})np$ with the higher n can be ignored.

In order to analyze the contributions of the satellite states $\text{Ne}^+ ({}^{1,3}\text{P})np$ ($n = 3, 4, 5, 6, 7$), the ratio B refers to the proportion of the intensity to the total satellite states intensity, and is also listed in Table I, which is consistent with experimental results [45]. It should be mentioned that the difference between the intensity of Kiselev *et al.* [43] and ours as well as experimental results [45], the corresponding ratio B also have deviation. It is an interesting phenomenon, whether it is $\text{Ne}^+ ({}^3\text{P})$ or $\text{Ne}^+ ({}^1\text{P})$ series, the relative strength of the satellite states decreases approximately twice as n increases. This is mainly because the electron interaction between $2p$ and np ($n = 3, 4, 5, 6, 7$) orbits becomes weaker and weaker with the increase of n . In Fig. 2, the probability density of $2p$ and shakeup orbitals np ($n = 3, 4, 5, 6, 7$) are shown. One can find that the density of orbitals np will move to larger r region with the increase in n , resulting in the decrease of the overlap of $2p$ with np ; thus, the form of satellite states $1s^{-1}2p^{-1}3p$ is the strongest shakeup channel. There is little difference between the probability density of $2p$ and np orbital ($n = 3, 4, 5, 6, 7$) for satellite states $\text{Ne}^+ ({}^1\text{P})np$ and $\text{Ne}^+ ({}^3\text{P})np$, so as shown in Table I, the intensities of $\text{Ne}^+ ({}^1\text{P})np$ ($n = 3, 4, 5, 6, 7$) are close to that of triplet-state $\text{Ne}^+ ({}^3\text{P})np$.

B. Single Auger decay of satellite states

In order to clearly illustrate the Auger transition process, the energy levels of Ne ions are presented in Fig. 3. Since the energy positions of satellite states are much higher than

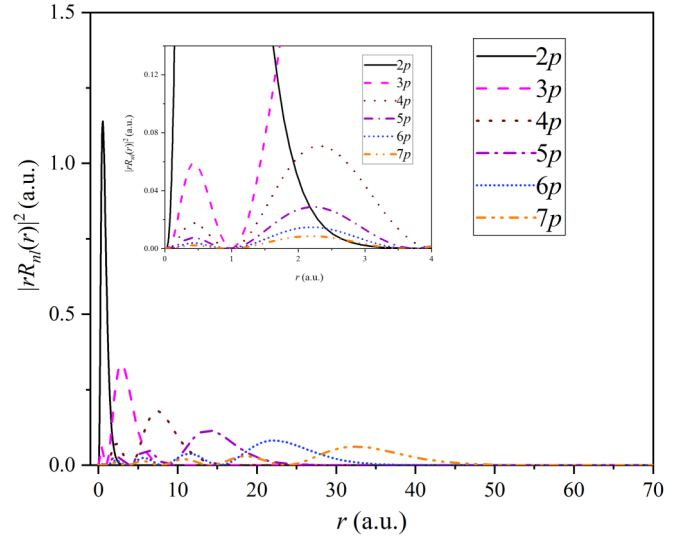


FIG. 2. The probability density of electrons of $2p$ (black and solid line), $3p$ (magenta and dashed line), $4p$ (wine and dotted line), $5p$ (purple and dashed-dotted line), $6p$ (blue and short dotted line), and $7p$ (orange and dashed-dotted-dotted line) orbital for satellite states $\text{Ne}^+ 1s^{-1}2p^{-1}np$ ($n = 3, 4, 5, 6, 7$).

the corresponding ions, they can be decayed by direct or cascade Auger process. The main configuration of final states for the Auger decay process is marked in different colors. It is important to study the SA transition process of satellite states, which will directly affect the results of multiple Auger decay processes. The orbital wave functions are obtained by optimizing main configuration $\text{Ne}^+ 1s^{-1}2p^{-1}3p$ and $2p^{-2}$, $2s^{-1}2p^{-1}$ of Ne^{2+} ion by using self-consistent procedures, respectively. In the CI calculation, the large-scale CSFs are produced by SD excitations from the main configuration to the orbitals $3s$, $3p$, $3d$, $4s$, and $4p$ separately. In order to consider the further Auger transition process, some important configurations $1s^{-1}2p^{-1}nl$, $1s^{-1}2s^{-1}nl$ for Ne^+ ions and $2p^{-3}nl$, $2s^{-1}2p^{-2}nl$,

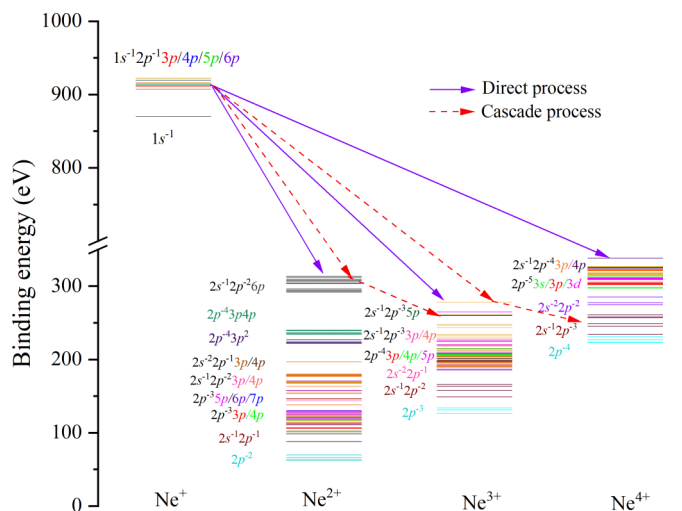


FIG. 3. Energy level diagram for Ne ions. Different Auger decay processes from satellite states $\text{Ne}^+ 1s^{-1}2p^{-1}np$ ($n = 3, 4, 5, 6$) are presented.

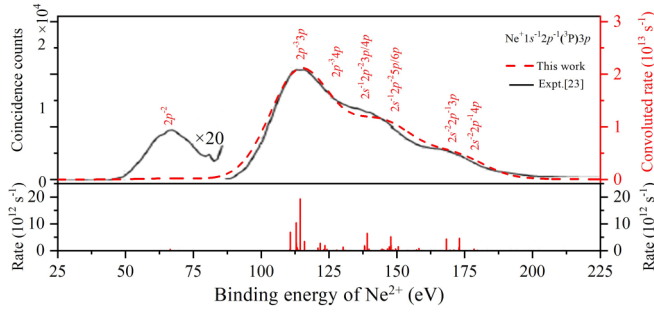


FIG. 4. The single Auger electron spectra of satellite states $\text{Ne}^+ 1s^{-1} 2p^{-1} ({}^3\text{P}) 3p$. The theoretical results are obtained by convolving the rates with a Gaussian profile of 15-eV FWHM for Auger electron around 900 eV to compare with experimental ones [23]. The main transition rates are represented by vertical solid lines in the bottom.

$2s^{-2} 2p^{-1} nl$ ($nl = 4d, 5s, 5p, 6s, 6p, 7s, 7p$) for Ne^{2+} ions are added, respectively. In addition, the biorthogonal conversion is also performed for the initial and final states of multiple Auger decay. The wave functions of Ne^{3+} and Ne^{4+} ions are obtained by using the similar optimization method described above for Ne^{2+} ions. For example, the reference configurations $2p^{-3}$, $2s^{-1} 2p^{-2}$ are considered for Ne^{3+} ions, and the addition configurations $[2s, 2p]^{-4} nl$ ($nl = 4d, 5s, 5p, 6s, 6p, 7s, 7p$) are included.

Since the ratio B of different initial states is considered in Table I, we declare that A_{nm}^1 means the rate of SA decayed from initial state n to final state $\text{Ne}^{2+} m$, where $n = 1, 2, 3$ represent the initial satellite states $\text{Ne}^+ ({}^3\text{P}) 3p$, $\text{Ne}^+ ({}^1\text{P}) 3p$ and $\text{Ne}^+ ({}^1\text{P}) 4p$, respectively. At the same time, to describe the contributions of the final states, the corresponding normalized decay rates \bar{A}_{nm}^1

$$\bar{A}_{nm}^1 = A_{nm}^1 / A_n^1(\text{total})$$

are also obtained, where $A_n^1(\text{total})$ represents the total SA rates decayed from satellite states n . The SA transition rates of satellite states $\text{Ne}^+ ({}^3\text{P}) 3p$ are indicated by the solid vertical lines, which correspond to the important states of Ne^{2+} that are marked in Fig. 4. The SA decay spectra were obtained by convolving the rates with a Gaussian profile of 15-eV FWHM for Auger electron around 900 eV, which are consistent with the experimental measurements in energy positions and relative intensities [23]. In order to analyze the SA electron spectrum in detail, the rates A_{nm}^1 , normalized rates \bar{A}_{nm}^1 , and the BR_1^1 for different processes of the important final states decayed from satellite states $\text{Ne}^+ ({}^3\text{P}) 3p$ are shown in Table II. For the SA of satellite states $\text{Ne}^+ ({}^3\text{P}) 3p$, the $\text{Ne}^{2+} 2p^{-3} 3p$ states around 110 to 116 eV are formed mainly by the spectator process with contributions of 26.79%. The states $2s^{-1} 2p^{-2} 3p$ are also produced by the spectator process with the proportion of 15.66%. As the most important transition, the rate of final states $\text{Ne}^{2+} 2p^{-3} 3p$ is $2.6 \times 10^{13} \text{ s}^{-1}$. In Table II, satellite states $\text{Ne}^+ ({}^3\text{P}) 3p$ decay into states $(2s2p)^{-3} 3p$ resulting from spectator process with accounting for 54.73%. Due to the interaction with $\text{Ne}^{2+} 2p^{-3} 3p$, the $2p^{-3} 4p$ states with the rate $2.2 \times 10^{13} \text{ s}^{-1}$ are another important decay channel accounting for 22.96%

TABLE II. The single Auger rates (A_{lm}^1) and corresponding normalized decay rates (\bar{A}_{lm}^1) from satellite states $\text{Ne}^+ 1s^{-1} 2p^{-1} ({}^3\text{P}) 3p$ to main final states $\text{Ne}^{2+} (m)$ are listed. The branching ratios (BR_1^1) of different processes are also shown. The number in the parentheses represents the powers of 10.

| Ne^{2+} state (m) | A_{lm}^1 | \bar{A}_{lm}^1 | $\text{BR}_1^1(\text{Process})$ |
|--------------------------------|------------|------------------|---------------------------------|
| $2p^{-2}$ | 2.7(10) | 0.03 | 0.04 (Participant) |
| $2s^{-1} 2p^{-1}$ | 8.2(9) | 0.01 | |
| $2p^{-3} 3s$ | 7.1(9) | 0.01 | 0.01 (Shakedown) |
| $2p^{-3} 3p$ | 2.6(13) | 26.79 | 54.73 (Spectator) |
| $2s^{-1} 2p^{-2} 3p$ | 1.5(13) | 15.66 | |
| $2s^{-2} 2p^{-1} 3p$ | 5.8(12) | 5.91 | |
| $2p^{-4} 3p^2$ | 4.8(12) | 4.87 | |
| $2p^{-4} 3p 4p$ | 1.5(12) | 1.50 | |
| $2p^{-3} 4p$ | 2.2(13) | 22.96 | 45.22 (Shakeup) |
| $2s^{-1} 2p^{-2} 4p$ | 1.1(13) | 11.48 | |
| $2s^{-2} 2p^{-1} 4p$ | 6.5(11) | 0.66 | |
| $2p^{-3} 5p$ | 3.7(12) | 3.83 | |
| $2s^{-1} 2p^{-2} 5p$ | 1.1(12) | 1.08 | |
| $2p^{-3} 6p$ | 3.2(12) | 3.24 | |
| $2s^{-1} 2p^{-2} 6p$ | 1.9(12) | 1.98 | |
| Total | 1.1(14) | 100 | 100 |

among 117 to 125 eV. In addition, the contribution of shakeup $2s^{-1} 2p^{-2} 3p \rightarrow 2s^{-1} 2p^{-2} 4p$ process is 11.48% shows that the shakeup processes are also important. The $2p^{-3} 5p$ and $2p^{-3} 6p$ states are also produced by the shakeup process accounting for 3.83 and 3.24%, respectively. The shakeup processes to the np ($n = 4, 5, 6$) orbital with that of 45.22%, which indicates significance of SA from satellite states $\text{Ne}^+ ({}^3\text{P}) 3p$. In addition, the BRs of $2p^{-2}$ and $2s^{-1} 2p^{-1}$ states generated by the participant process are weak with only 0.04%, which are smaller than the experimental measurements as shown in Fig. 4. It should be noted that those experimental intensities mainly come from valence photoionization [47]. As shown in Fig. 3, the final states $2s^{-2} 2p^{-1} 3p$ and $2s^{-2} 2p^{-1} 4p$ above the ionization threshold can be mainly ionized by further cascade process.

There is a strong interaction between satellite states $\text{Ne}^+ ({}^1\text{P}) 3p$ and $\text{Ne}^+ ({}^3\text{P}) 4p$ with a small energy interval, which makes the decay process difficult to distinguish in the experiment. In order to compare with the experimental SA spectra [23] containing the contribution of satellite states $\text{Ne}^+ ({}^1\text{P}) 3p$ and $\text{Ne}^+ ({}^3\text{P}) 4p$, the theoretical SA spectra are shown in Fig. 5(a). The individual SA spectra of the satellite states $\text{Ne}^+ ({}^1\text{P}) 3p$ and $\text{Ne}^+ ({}^3\text{P}) 4p$ are presented in Fig. 5(b). The $2p^{-3} 3p$ states around 110–116 eV are mainly formed from the spectator decay of satellite states $\text{Ne}^+ ({}^1\text{P}) 3p$, shown as the orange-dashed line at Fig. 5(b), while final states $2p^{-3} 4p$ among 117–125 eV produced by the spectator decay of the $\text{Ne}^+ ({}^3\text{P}) 4p$, which can be seen in the purple-dotted line in Fig. 5(b). By comparing panel (a) with panel (b) of Fig. 5, we can obtain that the contribution among 125–137 eV is mainly from the spectator decay of $\text{Ne}^+ ({}^3\text{P}) 4p$ states. As shown in Table III, the large branching ratios BR_2^1 of 55.0 and 41.42% of $(2s2p)^{-3} 4p$ states and $(2s2p)^{-3} 3p$ reveal the importance of the spectator process for the SA decay of $\text{Ne}^+ ({}^1\text{P}) 3p$ and $\text{Ne}^+ ({}^3\text{P}) 4p$. The rates of $2p^{-3} 3p$ states are $2.7 \times 10^{13} \text{ s}^{-1}$, resulting

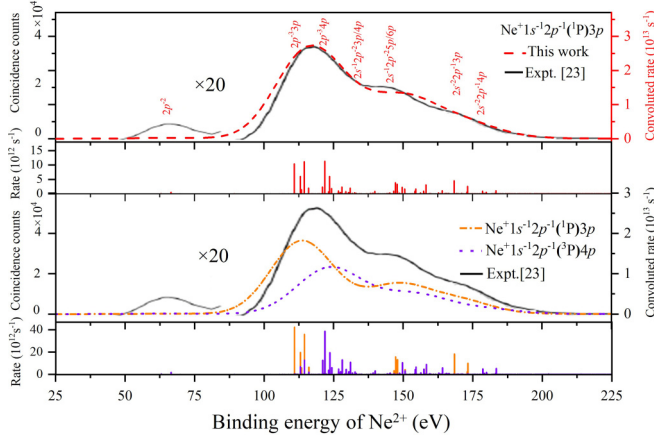


FIG. 5. The single Auger decay spectra containing the contribution from satellite states $\text{Ne}^+ 1s^{-1}2p^{-1}(^1\text{P})3p$ and $\text{Ne}^+ 1s^{-1}2p^{-1}(^3\text{P})4p$ in (a) for comparing with the experimental spectra [23]. The individual contribution is shown as orange-dashed line and purple-dotted line in (b), respectively. The theoretical results are obtained by convolving the rates with a Gaussian profile of 15-eV FWHM for Auger electron around 900 eV. The transition rates are represented by vertical solid lines in the bottom of (a) and (b).

in the \bar{A}_{2m}^1 of 19.78%, which decayed from the spectator process of the SA decay for $\text{Ne}^+ (^1\text{P})3p$. It should be mentioned that due to the spectator process of states $\text{Ne}^+ (^3\text{P})4p$, the transition to $2p^{-3}4p$ states is also important with the rate of $4.6 \times 10^{13} \text{ s}^{-1}$. Since the spectator processes make main contributions, the positions of the main peaks are different for the initial state $\text{Ne}^+ (^1\text{P})3p$ and $\text{Ne}^+ (^3\text{P})4p$. Like the SA decay process of $\text{Ne}^+ (^3\text{P})3p$ state, the participator process is also small, and the BR_2^1 of $2p^{-2}$, $2s^{-1}2p^{-1}$ states is only 0.03%. In addition, the shakeup ($3p/4p \rightarrow 5p, 6p$) process is also

TABLE III. The single Auger rates (A_{2m}^1) and corresponding normalized decay rates (\bar{A}_{2m}^1) from satellite states $\text{Ne}^+ 1s^{-1}2p^{-1}(^1\text{P})3p$ and $\text{Ne}^+ 1s^{-1}2p^{-1}(^3\text{P})4p$ to main final states $\text{Ne}^{2+} (m)$ are listed. The branching ratios (BR_2^1) of different processes are also shown. The number in the parentheses represents the powers of 10.

| Ne^{2+} state (m) | A_{2m}^1 | \bar{A}_{2m}^1 | BR_2^1 (Process) |
|--------------------------------|------------|------------------|---------------------------|
| $2p^{-2}$ | 3.3(10) | 0.02 | 0.03 (Participator) |
| $2s^{-1}2p^{-1}$ | 1.1(10) | 0.01 | |
| $2p^{-3}3s$ | 2.3(10) | 0.02 | 41.42 (Spectator-3p) |
| $2p^{-3}3p$ | 2.7(13) | 19.78 | |
| $2s^{-1}2p^{-2} 3p$ | 1.1(13) | 7.84 | |
| $2s^{-2}2p^{-1} 3p$ | 1.1(13) | 8.29 | |
| $2p^{-4}3p^2$ | 4.2(12) | 3.13 | |
| $2p^{-4}3p4p$ | 3.2(12) | 2.36 | |
| $2p^{-3}4p$ | 4.6(13) | 34.02 | 55.00 (Spectator-4p) |
| $2s^{-1}2p^{-2} 4p$ | 1.8(13) | 13.53 | |
| $2s^{-2}2p^{-1} 4p$ | 9.9(12) | 7.46 | |
| $2p^{-3}5p$ | 3.0(12) | 2.22 | 3.55 (Shakeup) |
| $2s^{-1}2p^{-2} 5p$ | 1.7(11) | 0.12 | |
| $2p^{-3}6p$ | 9.8(11) | 0.73 | |
| $2s^{-1}2p^{-2} 6p$ | 6.5(11) | 0.48 | |
| Total | 1.3(14) | 100 | 100 |

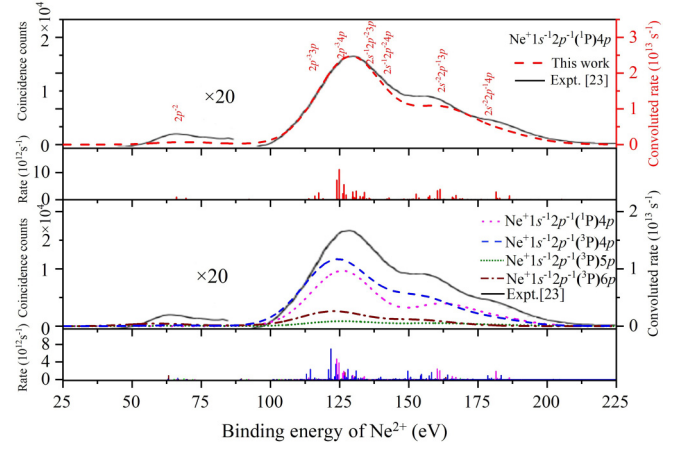


FIG. 6. The single Auger decay spectra containing the contributions of satellite states $\text{Ne}^+ 1s^{-1}2p^{-1}(^1\text{P})4p$ and $\text{Ne}^+ 1s^{-1}2p^{-1}(^3\text{P})np$ ($np = 4p, 5p, 6p$) in (a) for comparing with the experimental spectra [23]. The individual contribution is shown as blue-dashed line, purple-dotted line, gray-dashed-dotted line, and green-short dotted line in (b), respectively. The theoretical results are obtained by convolving the rates with a Gaussian profile of 15-eV FWHM for Auger electron around 900 eV. The transition rates are represented by vertical solid lines in the bottom of (a) and (b).

another essential channel, which can be found in Table III. It is stated here that in the subsequent discussion of this article, satellite states $\text{Ne}^+ (^1\text{P})3p$ include the contribution of satellite states $\text{Ne}^+ (^3\text{P})4p$ by default.

Similarly, due to the interaction among the satellite states, it is difficult to obtain SA decay spectra containing only satellite states $\text{Ne}^+ (^1\text{P})4p$ in experiments. The contributions of the satellite states $\text{Ne}^+ (^1\text{P})4p$, $\text{Ne}^+ (^3\text{P})4p$, $\text{Ne}^+ (^3\text{P})5p$, and $\text{Ne}^+ (^3\text{P})6p$ are included in the SA decay spectrum for comparing with the experimental spectra [23] in Fig. 6(a). As shown in Fig. 6(b), the individual SA spectra of these satellite states are presented as purple-dotted line, blue-dashed line, green-short dotted line, and gray-dashed-dotted line, respectively. Since $\text{Ne}^+ (^3\text{P})4p$ and $\text{Ne}^+ (^1\text{P})4p$ states have the same valence electron, the positions of the main peaks of SA electron spectrum are almost the same, and the difference of SA transition rates between them is mainly caused by the different intensity. As shown in Table IV, the \bar{A}_{3m}^1 of 36.92% for $2p^{-3}4p$ states is approximately seven times greater than that of the $2p^{-3}3p$ state produced by the shakedown process, which only accounts for 5.19%. The spectator processes leading to the final states $2p^{-3}4p$ and $2s^{-2}2p^{-1}4p$ are favored with the rates of $3.9 \times 10^{13} \text{ s}^{-1}$ and $1.1 \times 10^{13} \text{ s}^{-1}$, respectively. The SA decay rates of the satellite states $\text{Ne}^+ (^3\text{P})5p$ and $\text{Ne}^+ (^3\text{P})6p$ are almost negligible, which is due to the extremely small intensities. In addition, the intensities of the $2p^{-2}$, $2s^{-1}2p^{-1}$ states, which are mainly from the participator process of satellite states, are also small with the BR_3^1 of 1.1%. Similar to the above statement, the satellite states $\text{Ne}^+ (^1\text{P})4p$ include the contribution of satellite states $\text{Ne}^+ (^3\text{P})np$ ($n = 4, 5, 6$) by default in the subsequent discussion of this article. The major SA decay process of $\text{Ne}^+ (^1,^3\text{P})np$ ($n = 3, 4$) can be described as a spectator process where valence electrons do not participate in

TABLE IV. The single Auger rates (A_{3m}^1) and corresponding normalized decay rates (\bar{A}_{3m}^1) from satellite states $\text{Ne}^+ 1s^{-1}2p^{-1}(^1\text{P})4p$ containing contributions of $\text{Ne}^+ 1s^{-1}2p^{-1}(^3\text{P})np$ ($np = 4p, 5p, 6p$) to main final states $\text{Ne}^{2+}(m)$ are listed. The branching ratios (BR_3^1) of different processes are also shown. The number in the parentheses represents the powers of 10.

| Ne^{2+} state (m) | A_{3m}^1 | \bar{A}_{3m}^1 | BR_3^1 (Process) |
|--------------------------------|------------|------------------|---------------------------|
| $2p^{-2}$ | 9.0(11) | 0.85 | 1.10 (Participant) |
| $2s^{-1}2p^{-1}$ | 2.2(11) | 0.20 | |
| $2p^{-3}3s$ | 1.3(10) | 0.01 | 39.40 (Shakedown) |
| $2p^{-3}3p$ | 5.5(12) | 5.19 | |
| $2s^{-1}2p^{-2}3p$ | 1.7(13) | 15.92 | |
| $2s^{-2}2p^{-1}3p$ | 7.9(12) | 7.38 | |
| $2p^{-4}3p^2$ | 5.4(12) | 5.08 | |
| $2p^{-4}3p4p$ | 6.2(12) | 5.86 | |
| $2p^{-3}4p$ | 3.9(13) | 36.92 | 49.70 (Spectator) |
| $2s^{-1}2p^{-2}4p$ | 2.8(12) | 2.63 | |
| $2s^{-2}2p^{-1}4p$ | 1.1(13) | 10.07 | |
| $2p^{-3}5p$ | 3.8(12) | 3.57 | 9.80 (Shake-up) |
| $2s^{-1}2p^{-2}5p$ | 3.3(11) | 0.31 | |
| $2p^{-3}6p$ | 3.8(12) | 3.56 | |
| $2s^{-1}2p^{-2}6p$ | 2.6(12) | 2.43 | |
| Total | 1.0(14) | 100 | 100 |

the Auger decay process. Therefore, the main peak of the SA decay spectrum shifts to the direction of increasing binding energy in Figs. 4–6. The shakedown processes decayed to $2p^{-3}3s$ states are all weak with accounting for 0.01, 0.02, and 0.01%, respectively, as shown in Tables II–IV.

C. Double Auger decay of satellite states

Because the spectator processes are dominated by the SA decay of satellite states, there is a high probability that the final states of Ne^{2+} are autoionizing states, which makes the cascade process primary. The spectrum of the CDA is presented, which agrees with experimental results [23] in Fig. 7. The important peaks represent the $2p^{-3}$ states around 130 eV and the $2s^{-1}2p^{-2}$ states around 150 eV, respectively, formed by the participant process. The rates A_{nk}^2 and normalized rates \bar{A}_{nk}^2 of major transition channels for the CDA process are given in Table V, where A_{nk}^2 and \bar{A}_{nk}^2 ($n = 1, 2, 3$) represent rates and normalized rates for CDA process decayed by the initial states $\text{Ne}^+ (^3\text{P})3p$, $\text{Ne}^+ (^1\text{P})3p$, and $\text{Ne}^+ (^1\text{P})4p$, respectively. The transition rates of the main final state $2p^{-3}^2\text{P}_{3/2}$ are $1.5 \times 10^{13} \text{ s}^{-1}$ and $1.3 \times 10^{13} \text{ s}^{-1}$, which come from the decay processes of $\text{Ne}^+ (^3\text{P})3p$ and $\text{Ne}^+ (^1\text{P})3p$, respectively. For the decay process of initial states $\text{Ne}^+ (^1\text{P})4p$, the $2p^{-3}^4\text{S}_{3/2}$ is the most important transition channel and its transition rate is $1.6 \times 10^{13} \text{ s}^{-1}$. In addition, the rates of the $2s^{-1}2p^{-2}^2\text{S}_{1/2}$ states decayed from satellites states $\text{Ne}^+ (^3\text{P})3p$ and $\text{Ne}^+ (^1\text{P})3p$ are $1.1 \times 10^{13} \text{ s}^{-1}$ and $1.0 \times 10^{13} \text{ s}^{-1}$, respectively, which are also dominated transition by the participant process, while for the satellites states $\text{Ne}^+ (^1\text{P})4p$, the participant process to states $2s^{-1}2p^{-2}^2\text{P}_{1/2}$ is another important decay channel corresponding to the rate $9.3 \times 10^{13} \text{ s}^{-1}$. It can be concluded that the main decay channel is determined by the

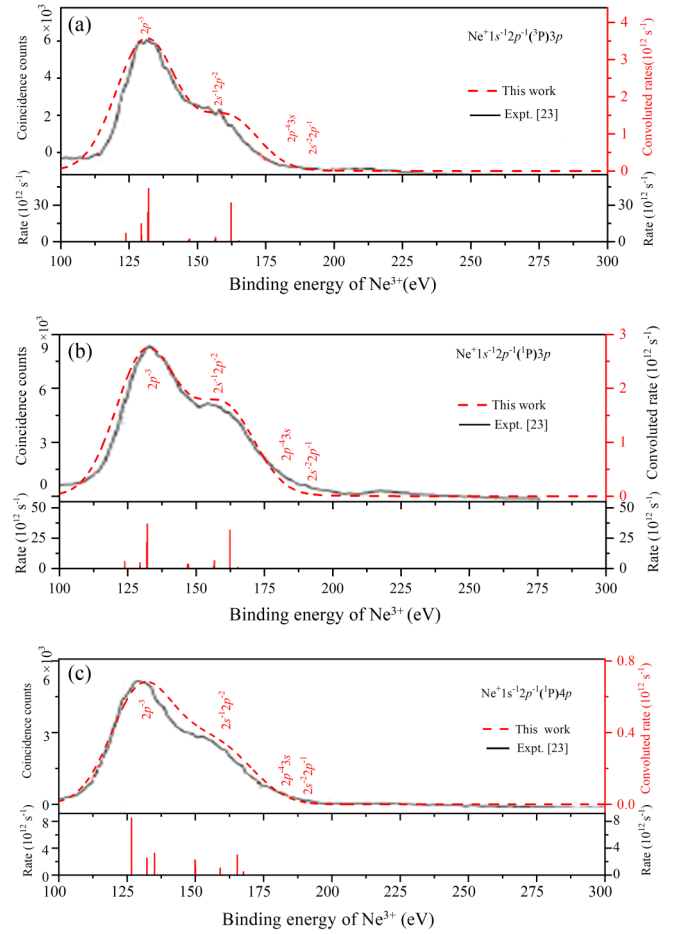


FIG. 7. The cascade double Auger spectra of satellite state $\text{Ne}^+ 1s^{-1}2p^{-1}(^3\text{P})3p$, $\text{Ne}^+ 1s^{-1}2p^{-1}(^1\text{P})3p$, and $\text{Ne}^+ 1s^{-1}2p^{-1}(^1\text{P})4p$ in (a), (b), and (c), respectively. The theoretical results (red-dashed line) are obtained by convolving the rates with a Gaussian profile of 13-eV FWHM for the Auger electron around 800 eV to compared with the experimental [23] results. The transition rates are represented by vertical solid lines in the bottom of (a)–(c), respectively.

valence electrons for the CDA process. For satellite states $\text{Ne}^+ (^3\text{P})3p$, $\text{Ne}^+ (^1\text{P})3p$, and $\text{Ne}^+ (^1\text{P})4p$, the \bar{A}_{nk}^2 (\bar{A}_{1k}^2 , \bar{A}_{2k}^2 , \bar{A}_{3k}^2) of k final states Ne^{3+} with greater than 175 eV are 0.2, 0.5, and 0.6%, respectively, we recognized that the further cascade process is extremely weak.

For the DDA process, only the KO mechanism is considered, since the total contribution of the SO process is two orders of magnitude smaller than the KO process. The DDA transition rates of satellite states $\text{Ne}^+ (^3\text{P})3p$, $\text{Ne}^+ (^1\text{P})3p$, and $\text{Ne}^+ (^1\text{P})4p$ are shown by vertical solid lines in Fig. 8, respectively. As result of the SA transitions decayed from initial state $\text{Ne}^+ (^1\text{P})4p$ being weaker than that of satellite states $\text{Ne}^+ (^3\text{P})3p$ and $\text{Ne}^+ (^1\text{P})3p$, its DDA processes are also weaker than these. The contributions of $2p^{-3}$, $2s^{-1}2p^{-2}$, and $2s^{-2}2p^{-1}$ states are small for DDA decay, while the $2p^{-4}np$ and $2s^{-1}2p^{-3}np$ states are main final states by the spectator process. Due to the spectator process mainly, the DDA decay from satellite states $\text{Ne}^+ (^1\text{P})4p$ to $\text{Ne}^{3+} 2p^{-4}3p$ is much smaller than that of decay from $\text{Ne}^+ (^1\text{P})3p$. The DDA spectra for $\text{Ne}^+ (^3\text{P})3p$ and $\text{Ne}^+ (^1\text{P})3p$ are slightly different from

TABLE V. The rates A_{nk}^2 , configurations of Ne^{3+} states k , angular momentum J , and the normalized decay rates $\bar{A}_{nk}^2 = A_{nk}^2/A_n^2(\text{total})$ ($n = 1, 2, 3$) are shown decayed from initial satellite states $\text{Ne}^+ ({}^3\text{P})3p$, $\text{Ne}^+ ({}^1\text{P})3p$, and $\text{Ne}^+ ({}^1\text{P})4p$ for CDA decay, respectively, where $A_n^2(\text{total})$ represent the total CDA rates. The number in parentheses represents the powers of 10.

| Ne^{3+} state (k) | J | $A_{1k}^2(\text{s}^{-1})$ | \bar{A}_{1k}^2 | $A_{2k}^2(\text{s}^{-1})$ | \bar{A}_{2k}^2 | $A_{3k}^2(\text{s}^{-1})$ | \bar{A}_{3k}^2 |
|---------------------------------|-----|---------------------------|------------------|---------------------------|------------------|---------------------------|------------------|
| $2p^{-3} ({}^4\text{S})$ | 3/2 | 2.3(12) | | 9.1(12) | | 1.6(13) | |
| $2p^{-3} ({}^2\text{D})$ | 5/2 | 5.0(12) | | 3.5(12) | | 5.1(12) | |
| $2p^{-3} ({}^2\text{D})$ | 3/2 | 1.9(12) | 68.1 | 2.8(12) | 61.3 | 5.3(12) | 59.6 |
| $2p^{-3} ({}^2\text{P})$ | 1/2 | 8.2(12) | | 8.3(12) | | 3.9(12) | |
| $2p^{-3} ({}^2\text{P})$ | 3/2 | 1.5(13) | | 1.3(13) | | 6.0(12) | |
| $2s^{-1}2p^{-2} ({}^4\text{P})$ | 5/2 | 3.8(11) | | 1.6(12) | | 1.7(12) | |
| $2s^{-1}2p^{-2} ({}^4\text{P})$ | 3/2 | 5.3(11) | | 1.8(12) | | 2.5(12) | |
| $2s^{-1}2p^{-2} ({}^4\text{P})$ | 1/2 | 7.2(11) | | 2.7(12) | | 2.3(12) | |
| $2s^{-1}2p^{-2} ({}^2\text{D})$ | 5/2 | 4.6(11) | | 1.5(12) | | 2.0(12) | |
| $2s^{-1}2p^{-2} ({}^2\text{D})$ | 3/2 | 1.2(12) | 31.7 | 4.2(12) | 37.2 | 2.9(12) | 39.8 |
| $2s^{-1}2p^{-2} ({}^2\text{S})$ | 1/2 | 1.1(13) | | 1.0(13) | | 2.6(12) | |
| $2s^{-1}2p^{-2} ({}^2\text{P})$ | 3/2 | 1.7(11) | | 1.7(11) | | 1.2(12) | |
| $2s^{-1}2p^{-2} ({}^2\text{P})$ | 1/2 | 2.0(11) | | 1.3(11) | | 9.3(12) | |
| Others | | 1.0(11) | 0.2 | 3.6(11) | 0.5 | 4.2(11) | 0.6 |
| Total | | 4.7(13) | 100 | 6.1(13) | 100 | 6.2(13) | 100 |

experimental measurement [23]. It is worth noting that the DDA transitions are weak, accounting for about 4%.

D. Triple Auger decay of satellite states

For the triple Auger (TA) process, the cascade and direct processes are also considered. In practical calculation, the step-by-step approximation method is also used to describe,

$$\text{Ne}^+(1s^{-1}2p^{-1}np) \xrightarrow{\text{DDA}} \text{Ne}^{3+} + 2e_A^- \xrightarrow{\text{Direct}} \text{Ne}^{4+} + 3e_A^- \text{ (DDD)}, \quad (11)$$

$$\text{Ne}^+(1s^{-1}2p^{-1}np) \xrightarrow{\text{DDA}} \text{Ne}^{3+*} + 2e_A^- \xrightarrow{\text{autoionization}} \text{Ne}^{4+} + 3e_A^- \text{ (DDC)}, \quad (12)$$

$$\text{Ne}^+(1s^{-1}2p^{-1}np) \xrightarrow{\text{CDA}} \text{Ne}^{3+} + 2e_A^- \xrightarrow{\text{Direct}} \text{Ne}^{4+} + 3e_A^- \text{ (CDD)}, \quad (13)$$

and

$$\text{Ne}^+(1s^{-1}2p^{-1}np) \xrightarrow{\text{CDA}} \text{Ne}^{3+*} + 2e_A^- \xrightarrow{\text{autoionization}} \text{Ne}^{4+} + 3e_A^- \text{ (CDC)}. \quad (14)$$

It should be mentioned that the contribution of the SO mechanism is far less than that of the KO mechanism; therefore, the transition rates of the DDD process can be expressed as

$$A_{\beta\delta\zeta}^3 = \sum_{\delta} A_{\beta\delta(DK)}^2 \int_0^{E_{\max}} \rho_{\beta\delta}(\varepsilon_0) \Omega_{\delta\zeta}(\varepsilon_0) d\varepsilon_0, \quad (15)$$

where the $A_{\beta\delta(DK)}^2$ denotes rate of DDA decay with KO mechanism as shown in the Eq. (7), $\Omega_{\delta\zeta}(\varepsilon_0)$ indicates collision intensity between intermediate Auger electrons and $|\psi_{\delta}^{3+}\rangle$ state. Because the probability of two intermediate Auger electrons simultaneously colliding with the state $|\psi_{\delta}^{3+}\rangle$ is extremely small, thus it is considered that one of the intermediate

Auger electrons interacts with the $|\psi_{\delta}^{3+}\rangle$ state by considering the energy distribution $\rho_{\beta\delta}(\varepsilon_0)$ in the actual calculation. $\rho_{\beta\delta}(\varepsilon_0)$ is the normalized distribution of energy for Auger electron [27,33] from 0 to E_{\max} . The E_{\max} is energies of Auger electron ionized from Ne^+ to Ne^{3+} .

In Eq. (12), the initial satellite state $\text{Ne}^+1s^{-1}2p^{-1}np$ decays to autoionization states of Ne^{3+*} by the DDA process with the KO mechanism. Because the energies of Ne^{3+*} states are higher than that of Ne^{4+} states, it will be further ionized through the autoionization process. The expression of the corresponding transition probability is

$$A_{\beta\delta\zeta}^3 = \sum_{\delta} A_{\beta\delta(DK)}^2 A_{\delta\zeta}^1 \Gamma_{\delta}^{-1}, \quad (16)$$

where Γ_{δ} represents the total decay lifetime of the intermediate $|\psi_{\delta}^{3+}\rangle$ states of Ne^{3+} .

In Eq. (13), the initial satellite state $\text{Ne}^+1s^{-1}2p^{-1}np$ decays to states of Ne^{3+} by CDA process and then decays to states of Ne^{4+} by the inelastic scattering process within the KO mechanism. The corresponding transition rate can be indicated as

$$A_{\beta\delta\zeta}^3 = \sum_{\delta} A_{\beta\delta(DC)}^2 \Omega_{\delta\zeta}(\varepsilon_0), \quad (17)$$

where $A_{\beta\delta(DC)}^2$ denotes the rate of the CDA process.

In Eq. (14), the TA decay can be decomposed into the CDA process and the subsequent autoionization. The corresponding rate of CDC process can be expressed as

$$A_{\beta\delta\zeta}^3 = A_{\beta\delta(DC)}^2 A_{\delta\zeta}^1 \Gamma_{\delta}^{-1}. \quad (18)$$

For the CDC process, the contributions of final states of Ne^{3+} with greater than ionization threshold are 0.2, 0.5, and 0.6%, respectively, which recognizes that the further cascade processes are extremely weak. In addition, the CDD process is prohibited, since the energy range of the second Auger electron is about 0–25 eV [48], which is less than the ionization threshold of 97.19 eV [49]. The DDD process can be

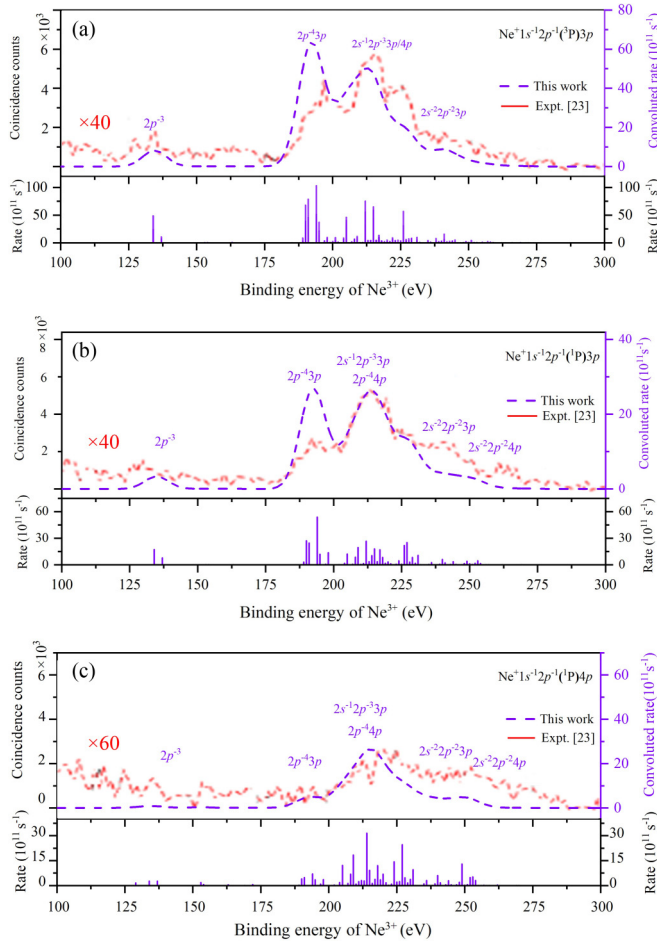


FIG. 8. The direct double Auger decay spectra of satellite states $\text{Ne}^+ 1s^{-1}2p^{-1}(^3\text{P})3p$, $\text{Ne}^+ 1s^{-1}2p^{-1}(^1\text{P})3p$, and $\text{Ne}^+ 1s^{-1}2p^{-1}(^1\text{P})4p$ in (a), (b), and (c), respectively. The theoretical spectra (purple-dashed line) are obtained convolving the rates with Gaussian profile of 10-eV FWHM for Auger electron around 600 eV to compare with experimental ones [23]. The transition rates are represented by vertical solid lines in the bottom of (a)–(c), respectively.

described as DDA decay and followed the inelastic scattering process; however, the transition rates are three orders of magnitude smaller than that of the DDC process, which can be ignored. For the TA process of satellite states, the DDC process is proved to be important; their spectra are shown and consistent with experimental measurement [23] in Fig. 9, and the states $\text{Ne}^{4+} 2p^{-4}$ are most important. While the intensity of $2s^{-1}2p^{-3}$ states with around 250 eV is slightly different from that of experiment [23], it should be mentioned that high-order ionization like TA decay is extremely weak; the absolute uncertainty caused by the observation system may be large [50].

E. Ion yields

In Table VI, the ion yields of Ne^{2+} , Ne^{3+} , and Ne^{4+} ions are provided for multiple Auger processes of satellite states $\text{Ne}^+ (^3\text{P})3p$, $\text{Ne}^+ (^1\text{P})3p$, and $\text{Ne}^+ (^1\text{P})4p$, which are in agreement with the experimental values [23], respectively. The yields of Ne^{2+} ions are greater than that of Ne^{3+} de-

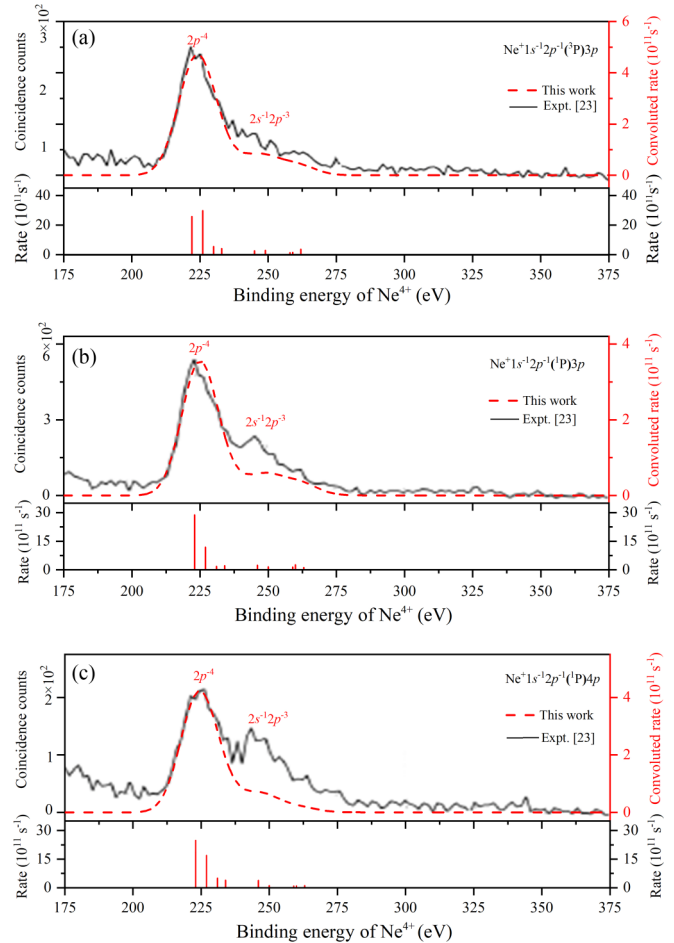


FIG. 9. The triple Auger decay spectra of satellite states $\text{Ne}^+ 1s^{-1}2p^{-1}(^3\text{P})3p$, $\text{Ne}^+ 1s^{-1}2p^{-1}(^1\text{P})3p$, and $\text{Ne}^+ 1s^{-1}2p^{-1}(^1\text{P})4p$ on (a)–(c), respectively. The theoretical spectra are obtained convolving rates with a Gaussian profile of 10-eV FWHM for Auger electron around 600 eV to compare with experimental ones [23]. The possible transition rates are represented by vertical solid lines in the bottom of (a)–(c), respectively.

cayed from the initial states $\text{Ne}^+ (^3\text{P})3p$ and $\text{Ne}^+ (^1\text{P})3p$ ($^1\text{P})3p$, which indicates that the SA process makes the main contribution, while DA decay is dominated for the Auger process of $\text{Ne}^+ (^1\text{P})4p$ states; thus, the yield of Ne^{3+} is greater than that of Ne^{2+} because the spectator processes are dominated leading to the main intermediate states with high-energy autoionizing states that can enhance the probability of the cascade process. Since the TA process is quite weak and the intensity of satellite states is much smaller than that of the main state, the absolute uncertainty of the observation system will have relatively large absolute uncertainty [50]. This is why our calculated ion yields 0.01, 0.02, and 0.02 are different from experimental results 0.02, 0.04, and 0.06 produced by the TA of satellite states $\text{Ne}^+ (^3\text{P})3p$, $\text{Ne}^+ (^1\text{P})3p$, and $\text{Ne}^+ (^1\text{P})4p$, respectively.

IV. CONCLUSIONS

For the photoionization-excitation processes, due to the rearrangement of electron density in the photoionization process

TABLE VI. The experimental [23] and calculated ion yields for the multiple Auger decay of satellite states $\text{Ne}^+ 1s^{-1}2p^{-1}(^3\text{P})3p$, $\text{Ne}^+ 1s^{-1}2p^{-1}(^1\text{P})3p$, and $\text{Ne}^+ 1s^{-1}2p^{-1}(^1\text{P})4p$, respectively.

| Ions | $\text{Ne}^+ (^3\text{P})3p$ | | $\text{Ne}^+ (^1\text{P})3p$ | | $\text{Ne}^+ (^1\text{P})4p$ | |
|------------------|------------------------------|------------|------------------------------|------------|------------------------------|------------|
| | This work | Expt. [23] | This work | Expt. [23] | This work | Expt. [23] |
| Ne^{2+} | 1 | 1 | 1 | 1 | 1 | 1 |
| Ne^{3+} | 0.71 | 0.57 | 0.73 | 0.65 | 1.60 | 1.52 |
| Ne^{4+} | 0.01 | 0.02 | 0.02 | 0.04 | 0.02 | 0.06 |

of $1s$ shell, the shakeup processes of valence electrons $2p \rightarrow (3p, 4p, 5p, 6p, 7p)$ are induced. It should be noted here that for comparison with the experimental results [45] the relative intensities (the photoionization cross section of $\text{Ne}^+ 1s^{-1}$ is normalized to 1) and ratio B of a series of satellite states $\text{Ne}^+ 1s^{-1}2p^{-1}(^3,^1\text{P})np$ ($n = 3, 4, 5, 6, 7$) are presented with photoionization-excitation spectrum. Furthermore, the multiple Auger decay processes of the major satellite states $\text{Ne}^+ (^3\text{P})np$ ($n = 3, 4$) have been investigated based on perturbation theory. The Auger decay rates, Auger electron spectrum, and ion yields of Ne^{2+} , Ne^{3+} , and Ne^{4+} are obtained and are in line with the experimental results [23].

For the SA decay process, the spectator processes are the main decay channels from the satellite states $\text{Ne}^+ (^3\text{P})3p$, $\text{Ne}^+ (^1\text{P})3p$, and $\text{Ne}^+ (^3\text{P})4p$. For CDA decay, the contributions of $2p^{-3}$ and $2s^{-1}2p^{-2}$ states formed by the participator process

are over 90%, while the $2p^{-4}np$ and $2s^{-1}2p^{-3}np$ states are the main final states which are formed by the spectator process for the DDA decay. It can be proven that the DDC process as shown in the Eq. (12) is important for the TA process of satellite states. Lastly, the spectator processes lead to the high-energy intermediate states that enhance the probability of the cascade process. Our results are also consistent with that of the experiment [23] and show the important influence of the valence electrons np .

ACKNOWLEDGMENTS

This work is supported by the National Key Research and Development Program of China (Grant No. 2017YFA0402300), and the National Natural Science Foundation of China (Grants No. 11774344 and No. 11474033).

- [1] Ch.Gerth, K. Tiedtke, M. Martins, B. Obst, P. Zimmermann, P. Glatzel, A. Verweyen, P. Wernet, and B. Sonntag, *J. Phys. B: At. Mol. Opt. Phys.* **31**, 2539 (1998).
- [2] S. H. Southworth, T. LeBrun, Y. Azuma, and K. G. Dyall, *J. Electron. Spectrosc. Relat. Phenom.* **94**, 33 (1998).
- [3] P. Saln, P. van der Meulen, H. T. Schmidt, R. D. Thomas, M. Larsson, R. Feifel, M. N. Piancastelli, L. Fang, B. Murphy, T. Osipov *et al.*, *Phys. Rev. Lett* **108**, 153003 (2012).
- [4] L. Fang, M. Hoener, O. Gessner, F. Tarantelli, S. T. Pratt, O. Kornilov, C. Buth, M. Guhr, E. P. Kanter, C. Bostedt *et al.*, *Phys. Rev. Lett* **105**, 083005 (2010).
- [5] B. Kanngießer, M. Jainz, S. Brünken, W. Bente, C. Gerth, K. Godehusen, K. Tiedtke, P. van Kampen, A. Tutay, and P. Zimmermann, *Phys. Rev. A* **62**, 014702 (2000).
- [6] D. Anin, S. M. Huttula, and M. Huttula, *J. Phys. B: At. Mol. Opt. Phys.* **46**, 175003 (2013).
- [7] W. Jitschin, R. Stötzel, T. Papp, and M. Sarkar, *Phys. Rev. A* **59**, 3408 (1999).
- [8] D. P. Spears, H. J. Fischbeck, and T. A. Carlson, *Phys. Rev. A* **9**, 1603 (1974).
- [9] P. H. Kobrin, S. Southworth, C. M. Truesdale, D. W. Lindle, U. Becker, and D. A. Shirley, *Phys. Rev. A* **29**, 194 (1984).
- [10] J. Schirmer, G. Angonoa, S. Svensson, D. Nordfors, and U. Gelius, *J. Phys. B: At. Mol. Phys.* **20**, 6031 (1987).
- [11] H. Schmoranzner, S. Lauer, F. Vollweiler, A. Ehresmann, V. L. Sukhorukov, B. M. Lagutin, I. D. Petrov, P. V. Demekhin, K.-H. Scharfner, B. Magel *et al.*, *J. Phys. B: At. Mol. Opt. Phys.* **30**, 4463 (1997).
- [12] T. Ishihara, J. Mizuno, and T. Watanabe, *Phys. Rev. A* **22**, 1552 (1980).
- [13] U. Gelius, *J. Electron. Spectrosc. Relat. Phenom.* **5**, 985 (1974).
- [14] B. Eriksson, S. Svensson, N. Mårtensson, and U. Gelius, *J. Phys. B: At. Mol. Opt. Phys.* **21**, 1371 (1988).
- [15] U. Becker, R. Wehlitz, O. Hemmers, B. Langer, and A. Menzel, *Phys. Rev. Lett* **63**, 1054 (1989).
- [16] R. Sankari, A. Kivimki, M. Huttula, T. Matila, H. Aksela, S. Aksela, M. Coreno, G. Turri, R. Camilloni, M. de Simone *et al.*, *Phys. Rev. A* **65**, 042702 (2002).
- [17] P. Declava, G. D. Alti, G. Fronzoni, and A. Lisini, *J. Phys. B: At. Mol. Opt. Phys.* **23**, 3777 (1990).
- [18] U. Becker and D. A. Shirley, *Phys. Scr.* **T31**, 56 (1990).
- [19] K. Jänkälä, R. Sankari, J. Schulz, M. Huttula, A. Cal, S. Heinsmki, S. Fritzsche, T. Rander, S. Svensson, S. Aksela *et al.*, *Phys. Rev. A* **73**, 022720 (2006).
- [20] K. Jänkälä, S. Urpelainen, M. Huttula, S. Fritzsche, S. Heinäsmäki, S. Aksela, and H. Aksela, *Phys. Rev. A* **77**, 062504 (2008).
- [21] L. Partanen, S. Fritzsche, K. Jänkälä, M. Huttula, S. Urpelainen, S. Osmekhin, H. Aksela, and S. Aksela, *Phys. Rev. A* **81**, 062513 (2010).
- [22] E. Andersson, S. Fritzsche, P. Linusson, L. Hedin, J. H. D. Eland, J. E. Rubensson, L. Karlsson, and R. Feifel, *Phys. Rev. A* **82**, 043418 (2010).
- [23] Y. Hikosaka, T. Kaneyasu, P. Lablanquie, F. Penent, and K. Ito, *Phys. Rev. A* **97**, 023405 (2018).

- [24] P. Linusson, S. Fritzsche, J. H. D. Eland, L. Hedin, L. Karlsson, and R. Feifel, *Phys. Rev. A* **83**, 023424 (2011).
- [25] M. Nakano, Y. Hikosaka, P. Lablanquie, F. Penent, S.-M. Huttula, I. H. Suzuki, K. Soejima, N. Kouchi, and K. Ito, *Phys. Rev. A* **85**, 043405 (2012).
- [26] K. Jänkälä, P. Lablanquie, L. Andric, M. A. Khalal, J. Palaudoux, F. Penent, J. M. Bizau, D. Cubaynes, S. Guilbaud, K. Ito *et al.*, *Phys. Rev. A* **101**, 023413 (2020).
- [27] Y. Ma, Z. Liu, F. Zhou, and Y. Qu, *Phys. Rev. A* **98**, 043417 (2018).
- [28] L. Liu, Y. Li, C. Gao, and J. Zeng, *Phys. Rev. A* **101**, 012507 (2020).
- [29] J. A. Tanis, J.-Y. Chesnel, F. Frémont, D. Hennecart, X. Husson, D. Lecler, A. Cassimi, J. P. Grandin, J. Rangama, B. Skogvall *et al.*, *Phys. Rev. A* **62**, 032715 (2000).
- [30] C. Buth, R. Beerwerth, R. Obaid, N. Berrah, L. S. Cederbaum, and S. Fritzsche, *J. Phys. B: At. Mol. Opt. Phys.* **51**, 055602 (2018).
- [31] I. P. Grant, Springer Ser. At., Opt., Plasma Phys. **40**, 1 (2007).
- [32] J. Bieroń, C. F. Fischer, S. Fritzsche, G. Gaigalas, I. P. Grant, P. Indelicato, P. Jönsson, and P. Pyykkö, *Phys. Scr.* **90**, 054011 (2015).
- [33] F. Zhou, Y. Ma, and Y. Qu, *Phys. Rev. A* **93**, 060501(R) (2016).
- [34] M. Y. Amusia, I. S. Lee, and V. A. Kilin, *Phys. Rev. A* **45**, 4576 (1992).
- [35] Y. Ma, F. Zhou, L. Liu, and Y. Qu, *Phys. Rev. A* **96**, 042504 (2017).
- [36] T. Schneider, P. L. Chocian, and J.-M. Rost, *Phys. Rev. Lett* **89**, 073002 (2002).
- [37] R. L. Simons and H. P. Kelly, *Phys. Rev. A* **22**, 625 (1980).
- [38] T. Pattard and J. Burgdörfer, *Phys. Rev. A* **63**, 020701(R) (2001).
- [39] J. L. Zeng, P. F. Liu, W. J. Xiang, and J. M. Yuan, *Phys. Rev. A* **87**, 033419 (2013).
- [40] P. Jönsson, X. He, C. F. Fischer, and I. P. Grant, *Comput. Phys. Commun.* **177**, 597 (2007).
- [41] S. Fritzsche, *Comput. Phys. Commun.* **183**, 1525 (2012).
- [42] M. F. Gu, *Can. J. Phys.* **86**, 675 (2008).
- [43] S. Fritzsche, K. Jänkälä, M. Huttula, S. Urpelainen, and H. Aksela, *Phys. Rev. A* **78**, 032514 (2008).
- [44] S. Stock, R. Beerwerth, and S. Fritzsche, *Phys. Rev. A* **95**, 053407 (2017).
- [45] N. Mårtensson, S. Svensson, and U. Gelius, *J. Phys. B: At. Mol. Phys.* **20**, 6243 (1987).
- [46] M. D. Kiselev, E. V. Gryzlova, S. M. Burkov, O. Zatsarinny, and A. N. Grum-Grzhimailo, *Atoms* **9**, 114 (2021).
- [47] Y. Hikosaka, P. Lablanquie, F. Penent, P. Selles, E. Shigemasa, and K. Ito, *Phys. Rev. A* **89**, 023410 (2014).
- [48] Y. Hikosaka, T. Aoto, P. Lablanquie, F. Penent, E. Shigemasa, and K. Ito, *J. Phys. B: At. Mol. Opt. Phys.* **39**, 3457 (2006).
- [49] A. Kramida, Yu. Ralchenko, and J. Reader, NIST ASD Team, NIST Atomic Spectra Database (ver. 5.9), National Institute of Standards and Technology (2022), <https://physics.nist.gov/asd>.
- [50] A. Muller, A. Borovik, Jr., T. Buhr, J. Hellhund, K. Holste, A. L. Kilcoyne, S. Klumpp, M. Martins, S. Ricz, J. Viefhaus *et al.*, *Phys. Rev. Lett* **114**, 013002 (2015).